Time-reversal symmetry protected chiral interface states between quantum spin and quantum anomalous Hall insulators

Huaqing Huang,[1] Zhaoyou Wang,[1] Nannan Luo,[1] Zhirong Liu,[2] Rong Lü,[1] Jian Wu,[1] and Wenhui Duan[1,3,4,*]

[1]*Department of Physics and State Key Laboratory of Low-Dimensional Quantum Physics, Tsinghua University, Beijing 100084, China*

[2]*College of Chemistry and Molecular Engineering, Peking University, Beijing 100871, China*

[3]*Collaborative Innovation Center of Quantum Matter, Tsinghua University, Beijing 100084, China*

[4]*Institute for Advanced Study, Tsinghua University, Beijing 100084, China*

(Received 10 July 2015; published 25 August 2015)

We theoretically investigate the electronic properties of the interface between quantum spin Hall (QSH) and quantum anomalous Hall (QAH) insulators. A robust chiral gapless state, which substantially differs from edge states of QSH or QAH insulators, is predicted at the QSH/QAH interface using an effective Hamiltonian model. We systematically reveal distinctive properties of interface states between QSH and single-valley QAH, multivalley high-Chern-number QAH and valley-polarized QAH insulators based on tight-binding models using the interface Green's function method. As an example, first-principles calculations are conducted for the interface states between fully and semihydrogenated bismuth (111) thin films, verifying the existence of interface states in realistic material systems. Due to the physically protected junction structure, the interface state is expected to be more stable and insensitive than topological boundary states against edge defects and chemical decoration. Hence our results of the interface states provide a promising route towards enhancing the performance and stability of low-dissipation electronics in real environment.

DOI: 10.1103/PhysRevB.92.075138 PACS number(s): 73.43.−f, 73.20.At

I. INTRODUCTION

Topological states (TSs) are new phases of quantum matter that are characterized by an insulating bulk but highly conducting (topologically protected) gapless boundary states [1–3]. In two dimensions, the quantum spin Hall (QSH) state has time-reversal (TR) symmetry protected gapless helical edge states on the boundary, where two states with opposite spin polarizations counterpropagate at a given edge [2,3]. While the quantum anomalous Hall (QAH) state has a topological protected chiral edge state where electric current flows unidirectionally along the edge of the sample without dissipation [1,4,5], similar to the well-known quantum Hall state [6]. Since the electron backscattering is expected to be prohibited, the edge channels of the QSH and QAH insulators conduct without dissipation. This property is robust against disorder scattering and other perturbation effects, and thus has promising potential applications in low-power-consumption electronic and spintronic devices.

It was recently demonstrated that gapless states also exist at the interface of two topological insulators depending on their helicity, spin chirality, or mirror symmetry [7–11]. However, a systematic investigation of the interface between QSH and QAH states (QSH/QAH), which is scientifically interesting for a better understanding of the basic properties of topological interface states in relation to boundary conditions, is still lacking. On the other hand, the QSH/QAH interface is achievable in various topological materials, because QAH states can be realized from QSH insulators by breaking the TR symmetry via introducing the ferromagnetism. So far, various methods have been proposed to realize ferromagnetism in QSH insulators, which can, in principle, be classified into three groups. One group is to induce ferromagnetism in QSH insulators through magnetic doping [12–16]. For instance, the QAH effect has been experimentally observed in Cr-doped $(Bi,Sb)_2Te_3$ around 30 mK recently[16]. Due to unavoidable inhomogeneous doping or controllable δ-doping (modulation-doping) [17,18], quantum dots and domains of QAH insulators could be embedded into QSH insulators and vice versa. Another group is to drive the transition from QSH to QAH state by chemical decoration, for example, by depositing $3d$ or $5d$ transition-metal atoms on graphene [19–21] and silicene [22], or controlling the surface functionalization of stanene, germanene, and bismuth thin film with hydrogen or halide atoms [23–25]. By patterning surface passivation using a lithographic technique, which is feasible now in partially hydrogenated graphene nanostructures [26–28], one can control and even design the QSH/QAH interface in stanene and bismuth thin films. In addition, ferromagnetism in QSH insulators can also be induced due to the proximity coupling to magnetic insulators [29], e.g., by depositing graphene on the (111) surface of $BiFeO_3$ [30]. By etching the substrate just like that in integrated circuit fabrication before transferring QSH insulators onto it, one can also build an interface with different shapes. For the evaluation of the overall performance of TS-based electronic devices, it is highly important to explore the QSH/QAH interface.

Although the presence of topological edge states is guaranteed by the topological nature of the bulk electronic structure, the detailed behavior of edge states can be significantly affected by the boundary conditions. The native edges of topological materials suffer from the simultaneous presence of both trivial and nontrivial edge modes due to the local dangling bond states [31,32]. The roughness and unavoidable defects at edges also have a strong influence on the properties of edge states. Moreover, it has been reported that a small amount of chemical adsorption of gas molecules or spontaneous edge reconstruction can significantly modify the dispersion, Fermi velocity, spatial location of the Dirac point, spin texture,

*dwh@phys.tsinghua.edu.cn

and the Dirac cone anisotropy [33–36], which are important parameters of TS-based electronic devices. In contrast, the interface states sandwiched between two bulk materials are physically protected against those effects [37], which may be important in enhancing the stableness and insensitiveness of topological electronics.

In this work, we focus on the electronic states of the QSH/QAH interface. We show that there exists a robust chiral gapless state at the QSH/QAH interface, which is essentially different from both the chiral edge states of QAH insulators and the TR symmetry protected helical edge states of QSH insulators. The physical origin of the QSH/QAH interface states and their unique properties is demonstrated by theoretical analysis. Furthermore, we systematically investigate the interfaces between QSH and several kinds of QAH states, such as single-valley QAH, multivalley high-Chern-number QAH, and valley-polarized QAH states, using tight-binding models and first-principles calculations. We also illustrate the evolution of edge states when QSH and QAH insulators are brought close to each other so that their edges touch each other forming an interface. As the interface states are buried between bulk materials, we expect the interface state to be more stable and insensitive against various perturbations. Hence our studies of QSH/QAH interface states are not only of fundamental interest for basic science but also of crucial importance for controlling the performance and stability of topological electronics in real environment.

The paper is organized as follows. In Sec. II, we derive the general behavior of the QSH/QAH interface states. In Sec. III, we introduce the tight-binding models that will be used for illustrative calculations. We then show the materials system for first-principles calculations and the details of computational methods, as well as the interface Green's function approach used in modeling the interface between two semi-infinite systems. The numerical results are presented and discussed in Sec. IV, and we end with a summary in Sec. V.

II. THEORETICAL MODEL ANALYSIS

The simplest Hamiltonian of QSH insulator was first proposed by Bernevig, Hughes, and Zhang (BHZ) to describe the effective theory of the QSH effect and topological phase transition in HgTe/CdTe quantum wells [3]. The general form of the effective Hamiltonian is given by [3]

$$H_{\mathrm{BHZ}} = \begin{pmatrix} h(\mathbf{k}) & 0 \\ 0 & h^*(-\mathbf{k}) \end{pmatrix}, \tag{1}$$

where $\mathbf{k} = (k_x, k_y)$, $h(\mathbf{k}) = \epsilon(\mathbf{k}) + M(\mathbf{k})\sigma_z + A(k_x\sigma_x + k_y\sigma_y)$ and $\sigma_{x,y,z}$ are the Pauli matrices. $\epsilon(\mathbf{k})$ and $M(\mathbf{k})$ are expanded as $\epsilon(\mathbf{k}) = C - D(k_x^2 + k_y^2)$ and $M(\mathbf{k}) = M - B(k_x^2 + k_y^2)$. A, B, C, and D are parameters that depend on the material composition and structure. In particular, if M and B have the same sign (i.e., $MB > 0$), the system is topologically nontrivial, and a pair of helical edge states exist at the boundary between the QSH insulator and ordinary insulator or vacuum, where the counterpropagating edge states carry opposite spins. While the QAH insulator can be described by the BHZ Hamiltonian H_{BHZ} with an additional Zeeman-type of coupling

$$H_G = \mathrm{diag}(G_E, G_H, -G_E, -G_H), \tag{2}$$

where G_E and G_H describe the spin splitting of electron and hole bands, respectively, which are generically different [12,23]. This Zeeman-type term, which can be realized by exchange coupling with magnetic impurities, breaks the TR symmetry of the system. Liu *et al.* firstly proposed this Hamiltonian to predict the single-valley (around the Γ point) QAH state with Chern number $\mathcal{C} = 1$ in $Hg_{1-y}Mn_y$ Te/CdTe quantum wells [12]. The chiral edge state, which characterizes the QAH phase, is determined by the conditions [12]

$$(2M + G_E - G_H)(2M - G_E + G_H) < 0, \tag{3}$$

$$(2M + G_E + G_H)(2M - G_E - G_H) > 0. \tag{4}$$

We consider an interface at $y = 0$ between a QSH insulator ($y < 0$) and a QAH insulator ($y > 0$) [Fig. 1(b)]. The interface breaks the translational symmetry in the y direction, while the bulk periodicity parallel to the interface is preserved, then k_x is still a good quantum number. Note that the Hamiltonians are block-diagonal, so we study the upper and lower blocks separately. For simplicity, the overall energy shift term C in $\epsilon(\mathbf{k})$ is ignored. The upper block, $h(\mathbf{k})$, of the Hamiltonian for the left (H_L) and right (H_R) parts of the interface can be rewritten as follows:

$$H_L = \begin{pmatrix} M - B_+(k_x^2 - \partial_y^2) & A(k_x - \partial_y) \\ A(k_x + \partial_y) & -M + B_-(k_x^2 - \partial_y^2) \end{pmatrix} \tag{5}$$

and

$$H_R = \begin{pmatrix} S + M' - B_+(k_x^2 - \partial_y^2) & A(k_x - \partial_y) \\ A(k_x + \partial_y) & S - M' + B_-(k_x^2 - \partial_y^2) \end{pmatrix} \tag{6}$$

with $B_\pm = B \pm D$, $S = (G_E + G_H)/2$, and $M' = M + (G_E - G_H)/2$. According to previous investigation of edge states [38], we adopt the trial function $\Phi = \binom{\phi_1}{\phi_2} e^{\lambda y}$ for $y < 0$ region and get the secular equation with four roots $\pm\lambda_{1,2}$,

$$\lambda_{1,2}^2 = k_x^2 + F \pm \sqrt{F^2 - \theta^2}, \tag{7}$$

where $F(M,E) = \frac{A^2 - B_-(M-E) - B_+(M+E)}{2B_-B_+}$ and $\theta(M,E) = \sqrt{\frac{M^2 - E^2}{B_-B_+}}$. In order to have a bound state solution near the junction, we take the Dirichlet boundary condition in which the wave function must vanish at $y = \pm\infty$. Hence we chose the following basis for the $y < 0$ region:

$$\Phi_{1,2} = \begin{pmatrix} A(k_x - \lambda_{1,2}) \\ E - M + B_+(k_x^2 - \lambda_{1,2}^2) \end{pmatrix} e^{\lambda_{1,2} y}, \tag{8}$$

where $\mathrm{Re}(\lambda_{1,2}) > 0$. Similarly, for $y > 0$, we choose

$$\Psi_{1,2} = \begin{pmatrix} A(k_x + \lambda'_{1,2}) \\ E - S - M' + B_+(k_x^2 - {\lambda'_{1,2}}^2) \end{pmatrix} e^{-\lambda'_{1,2} y}, \tag{9}$$

with ${\lambda'}_{1,2}^2 = k_x^2 + F' \pm \sqrt{F'^2 - \theta'}$ and $\mathrm{Re}(\lambda'_{1,2}) > 0$, where $F' = F(M', E - S), \theta' = \theta(M', E - S)$.

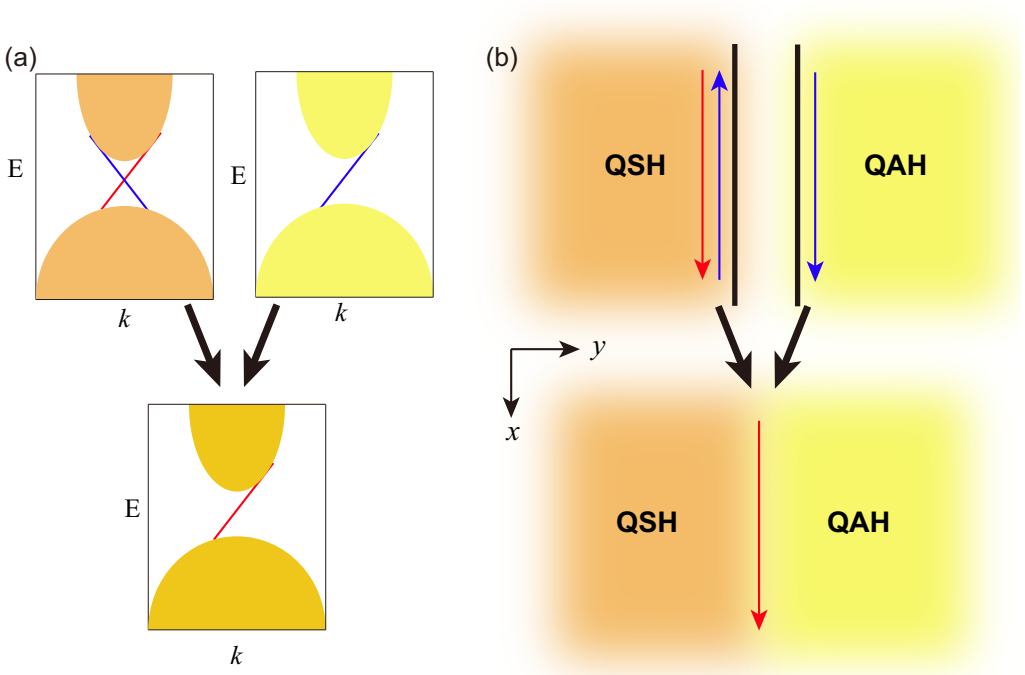

FIG. 1. (Color online) Schematics of the evolution of edge states in momentum space (a) and real space (b) when putting the QSH and QAH insulators together to form an interface. Red and blue colors represent different spin polarizations.

Assuming the solution of the interface state has a general form:

$$\psi = \begin{cases} C_1\Phi_1 + C_2\Phi_2, & y < 0 \\ C_1'\Psi_1 + C_2'\Psi_2, & y > 0 \end{cases}. \tag{10}$$

The wave function and its derivative should be continuous at $y = 0$,

$$\psi|_{y=0^+} = \psi|_{y=0^-},\ \partial_y\psi|_{y=0^+} = \partial_y\psi|_{y=0^-}. \tag{11}$$

Therefore the characteristic equation at $k_x = 0$ gives

$$\begin{aligned}&(\sqrt{F+\theta} + \sqrt{F'+\theta'})^2[(M'+S-E)\theta + (M-E)\theta'] \\ &\quad + \frac{BS - D(M'-M)}{B_- B_+}[(M'+S-E)\theta - (M-E)\theta'] \\ &\quad = 0.\end{aligned} \tag{12}$$

After some tedious calculations (for detailed derivations, see Appendix A), we find that when $MM' < 0$, Eq. (12) has a solution, i.e., a bound state near the junction exists. And there is no solution if $MM' > 0$. Similarly, we find that the existence condition of an interface state for the lower block is $MM'' < 0$ with $M'' = M - (G_E - G_H)/2$. In order to ensure that the system is always insulating, here we assume that S satisfies Eq. (4).

Combining the above conditions, we arrive that for the QSH/QAH interface, either $MM' < 0$, $MM'' > 0$ or $MM' > 0$, $MM'' < 0$ is valid according to Eq. (3), hence there must be a gapless interface state as shown in Fig. 1(a). However, we must make it clear that this interface state does not simply inherit from the chiral edge state of the QAH insulator since it has opposite spin polarization. This is not straightforward. To elucidate the issue, let us understand the physics from the edge state picture [Fig. 1(b)]. If $G_E < 0$ and $G_H > 0$, a spin-down gapless state exists at the edge of the QAH insulator. The backscattering is forbidden for the edge states of QAH and QSH insulators, because there is no state to be backscattered into. When the QAH and QSH insulators approach each other gradually, the spin-down edge state of the QAH insulator is destroyed due to the coupling to one of the helical edge states of the QSH insulator. The backscattering for the spin-down channel is allowed, hence gapless states of this channel are gapped, and eventually disappear, leaving only the spin-up edge state bound to the interface. Because the remaining interface state originates from the QSH insulator, it is topologically protected by TR symmetry, and is hence robust against structural disorder.

In more realistic QAH insulators, such as a multivalley QAH state with a high Chern number [39] and a valley-polarized QAH state [40,41], the number of chiral edge states is higher and the edge state becomes valley-contrasting spin polarized. Hence the detailed behavior of interface states would be much more complicated. However, as long as the edge states of QSH and QAH insulators couple to each other at the interface and the whole heterostructure remains insulating, the difference in topology of bulk band structures guarantees the existence of interface states. Therefore it is expected that the QSH/QAH interface states always exist and show some unique features different from the edge states of QSH or QAH insulators. Several typical examples will be presented in the following to illustrate the behaviors of interface states between QSH and various kinds of QAH insulators.

III. NUMERICAL CALCULATION

Although the above effective low-energy model analysis already gives a basic picture of the physical mechanism of the interface state, to obtain more quantitative understandings,

we preform realistic electronic structure calculations based on tight-binding (TB) models as well as a density-functional theory description of materials. In particular, we use a BHZ-type TB model to study the interface between a QSH and a single-valley QAH state with Chern number $\mathcal{C} = 1$, and the generalized Kane-Mele model to study the interface between a QSH insulator and a multivalley QAH insulator with a high Chern number ($\mathcal{C} = 2$) or a valley-polarized QAH insulator. These TB models are described in Sec. III A. We then compute the behavior of the interface in hydrogenated bismuth (111) thin films using first-principles calculations. The details of our computational approach are presented in Sec. III B. In order to investigate the interface between two semi-infinite systems, we adopt the interface Green's function methods which will be described in Sec. III C.

A. Tight-binding models

We first introduce a simplified TB model that captures all the essential symmetries and topology of the BHZ model. All the interesting low-energy physics occurs near the Γ point, and the unimportant behavior of band structures at high-energy can be ignored. Therefore we consider a four-band square lattice model which gives the Hamiltonian of the form of Eq. (1), with the matrix elements given by

$$\begin{aligned} h(\mathbf{k}) &= \epsilon(\mathbf{k}) + M(\mathbf{k})\sigma_z + A(\sin k_x \sigma_x - \sin k_y \sigma_x), \\ \epsilon(\mathbf{k}) &= C - 2D(2 - \cos k_x - \cos k_y), \\ M(\mathbf{k}) &= M - 2B(2 - \cos k_x - \cos k_y). \end{aligned} \tag{13}$$

Obviously, the lattice Hamiltonian can reduce to the BHZ one in Eq. (1) near the Γ point, thus this BHZ-type TB model can represent both QSH and a single-valley QAH state with $\mathcal{C} = 1$ if the additional Zeeman-type term H_G in Eq. (2) is added. Actually, in order to investigate the topological phase transition (TPT) from a QSH to a QAH state, we add αH_G into this model, and increase the factor α from 0 to 1 gradually. We adopt the values of parameters in Eq. (13) from Ref. [23] to simulate the interface between half-side and fully surface passivated stanene by halide atoms, which were predicted to be QAH and QSH insulators, respectively [23,42]. Note that other QSH/QAH interfaces, for example, an interface between HgTe/CdTe and $Hg_{1-y}Mn_y$ Te/CdTe quantum wells [3,12] can also be described by this model using different parameters.

The Kane-Mele model [2] for the QSH effect is a honeycomb lattice model with the TR invariant spin-orbit coupling (SOC). The low-energy bands form two valleys near the K and K' points at opposite corners of the hexagonal Brillouin zone. By adding extra terms such as an exchange field, several kinds of QAH states can be realized from the QSH state in this model. The generalized Kane-Mele model takes the form

$$\begin{aligned} H = & -t \sum_{\langle ij\rangle\mu} c^\dagger_{i\mu} c_{j\mu} + i\lambda_{\mathrm{SO}} \sum_{\langle\langle ij\rangle\rangle\mu\nu} \zeta_{ij} c^\dagger_{i\mu} \sigma^z_{\mu\nu} c_{j\nu} \\ & - i\lambda_{\mathrm{IR}} \sum_{\langle\langle ij\rangle\rangle\mu\nu} \xi_i c^\dagger_{i\mu} (\sigma \times \hat{\mathbf{d}}_{ij})^z_{\mu\nu} c_{j\nu} \\ & + i\lambda_{\mathrm{ER}} \sum_{\langle ij\rangle\mu\nu} c^\dagger_{i\mu} (\sigma \times \hat{\mathbf{d}}_{ij})^z_{\mu\nu} c_{j\nu} \\ & + \lambda_v \sum_i \xi_i c^\dagger_{i\mu} c_{i\mu} + M \sum_{i\mu\nu} c^\dagger_{i\mu} \sigma^z_{\mu\nu} c_{i\nu}, \end{aligned} \tag{14}$$

where $c^\dagger_{i\alpha}(c_{i\mu})$ is a creation (annihilation) operator for an electron with spin μ on site i. The first term represents the nearest-neighbor hopping with amplitude t. The second term describes the mirror symmetric SOC, which involves the next-nearest-neighbor hopping. $\zeta_{ij} = (2/\sqrt{3})(\hat{\mathbf{d}}_1 \times \hat{\mathbf{d}}_2)$, where $\hat{\mathbf{d}}_1$ and $\hat{\mathbf{d}}_2$ are unit vectors along the two bonds that connect the next-nearest-neighbor sites. The single (double) brackets label the nearest (next-nearest) neighbor pairs. μ and ν denote spin indices and σ are the spin Pauli matrices. The third and fourth terms are the intrinsic and extrinsic Rashba SOC terms, respectively. $\hat{\mathbf{d}}_{ij}$ represents the unit vector from site i to j, and $\xi_i = \pm 1$ for A and B sublattice. The last two terms correspond to a staggered sublattice potential and a uniform exchange field, which violate the twofold in-plane rotation and TR symmetries, respectively.

This Hamiltonian has been used to investigate possible topological phases, such as the QSH state [2], the multivalley QAH state with a high Chern number [39], and valley-polarized QAH states [40,41], in graphene and silicene. When the exchange field is absent (i.e., $M = 0$), the TR symmetry is preserved in this model. After including the SOC effect, a bulk band gap opens to host a TR symmetry-protected QSH state. In the QSH phase, a pair of dissipationless helical edge states with opposite spins exist, connecting the conduction and valance bands at different valleys [2]. Then, if we turn on the exchange field to break the TR symmetry of the system, a multivalley QAH phase with a high Chern number can be realized, where each valley provides a Chern number $\mathcal{C}_K = \mathcal{C}_{K'} = 1$ and the total Chern number $\mathcal{C} = \mathcal{C}_K + \mathcal{C}_{K'} = 2$ [39]. By further tuning the extrinsic Rashba SOC, the system is driven into the so-called valley-polarized QAH state [40,41], characterized by nonzero Chern number $\mathcal{C}$ and valley Chern number $\mathcal{C}_v \equiv \mathcal{C}_K - \mathcal{C}_{K'}$. In this phase, two valleys contribute to different Chern numbers, i.e., $\mathcal{C}_K = 1$ and $\mathcal{C}_{K'} = -2$. The imbalance of Chern number from different valleys gives rise to the valley-polarized QAH state with $\mathcal{C} = -1$ and $\mathcal{C}_v = 3$, which possesses the properties of both the QAH effect and the quantum valley Hall effect [40,41]. Hence by varying the relative strength of the parameters in Eq. (14), we can study the interfaces between QSH and different kinds of QAH states.

B. Material systems and computational methods

We take a single bilayer of hydrogenated Bi(111) film as an illustrative example to demonstrate the existence of gapless QSH/QAH interface states. A single Bi (111) bilayer forms a slightly buckled hexagonal lattice with two atoms per unit cell. According to previous studies [24,25], the full hydrogenated Bi (111) bilayer [denoted as H-Bi(111)] is a QSH insulator with bulk band gap as large as ∼1.0 eV. When the hydrogen atoms are removed from one side of H-Bi(111) while kept on the other side [semihydrogenated Bi (111) film, labeled by sH-Bi(111)], the system becomes a valley-polarized QAH insulator with a gap of ∼0.35 eV [24,25]. In the valley-polarized QAH state, the valley-resolved Chern numbers contributed from K and K' valleys are different, i.e., $\mathcal{C}_K = 1, \mathcal{C}_{K'} = 0$, and the corresponding total Chern and valley Chern numbers are $\mathcal{C} = \mathcal{C}_v = 1$. Hence the QSH/QAH interface can be achieved in the single Bi (111) bilayer by controlling the surface hydrogenation. For graphene, a precise control over the surface

hydrogenation is already feasible now, benefitting from recent experimental progress [26–28].

In order to investigate the H-Bi(111)/sH-Bi(111) interface, we carry out first-principles calculations based on density functional theory (DFT) as implemented in the Vienna *ab initio* simulation package [43] with the projector augmented-wave method. Perdew-Burke-Ernzerhof parametrization of the generalized gradient approximation is used for the exchange-correlation potential [44]. The plane-wave energy cutoff is set to 250 eV, and the Brillouin zone is sampled by a Γ-centered $12 \times 12 \times 1$ **k**-point mesh. The layer structures of H-Bi(111) and sH-Bi(111) are modeled with a vacuum region more than 10-Å thick to eliminate the spurious interaction between neighboring layers. After obtaining the self-consistent ground states of bulk H-Bi(111) and sH-Bi(111), we construct Wannier representations for these two material systems using the WANNIER90 package [45] and generate *ab initio* TB Hamiltonians from the DFT calculation [46]. It should be noted that the *ab initio* TB models are realistic in the sense that the Wannier interpolated band structures precisely reproduce the results of first-principles calculations [47]. Based on the effective TB Hamiltonian, we further calculate the interface state using the interface Green's function method as we will explain in Sec. III C.

C. Interface Green's function method

The Green's function method is a powerful approach to explore the electronic structure of a perfect crystal with translational symmetry, and can be used also in cases where the periodicity of the system is destroyed, e.g., as for surface/edge-terminated solids and interfaces. The surface Green's function, which is widely used in determining the topological-protected gapless boundary states of TSs [48,49], can be determined via highly efficient iterative methods [50] at a greatly reduced computational cost. In order to study the interface between two different materials, as in the system depicted in Fig. 2, we make use of the surface Green's function matching (SGFM) theory [51–53] to get the interface Green's function, from which all useful properties of the interface can be obtained. In the following, we will briefly introduce the surface Green's function method and the SGFM theory.

As is well known, any solid with a surface can be broken down into a semi-infinite stack of principal layers, such that only the nearest-neighbor interaction between adjacent principal layers exists. A principal layer may contain one or more atomic layers, depending on the geometry and on the range of interactions included in the model, and the crystal can be reproduced by translations of the principal layers. If the bulk periodicity parallel to the surface is preserved by all the atomic planes right up to the surface, then $k_\parallel$ is still a good quantum number. For each $k_\parallel$, the surface problem can be reduced to a one-dimensional chain in the direction perpendicular to the surface.

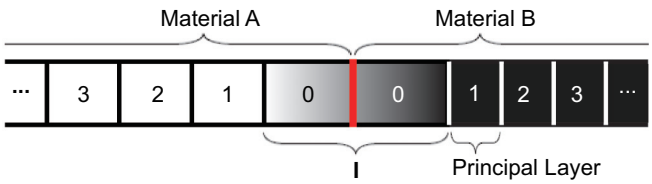

FIG. 2. (Color online) Schematic illustration of a system consisting of two semi-infinite materials. "I" denotes the interface region for which we need to calculate the Green's function G_I. Each semi-infinite system can be split into principal layers with Hamiltonian submatrices labeled according to the distance to the interface.

Within the principal layer approximation, the surface Green's function with fixed $k_\parallel$ can be written as

$$g(\epsilon,k_\parallel) = (\epsilon - H_{00} - H_{01}T)^{-1}, \tag{15}$$

where $\epsilon = E + i\eta$ with η arbitrarily small. H_{nm} are the matrix elements of the Hamiltonian between the layer orbitals, and the transfer matrix T is given by

$$T = (\epsilon - H_{00} - H_{01}T)^{-1}H_{01}^\dagger, \tag{16}$$

which can be computed self-consistently via an efficient iterative scheme proposed by López Sancho *et al.* [50]. It should be noted that in Eq. (16), we have made the simplifying but not essential assumption of an ideal surface, i.e., $H_{00} = H_{11} = \ldots$ and $H_{01} = H_{12} = \ldots$. In practice, we can also easily take various surface effects into account by simply modifying H_{00} and H_{01} in Eq. (15).

For an interface system consisting of two semi-infinite materials (see Fig. 2), let us discuss its electronic structure with the formulation of the matching problem in terms of the SGFM analysis. The interface Green's function G_I can be calculated from the bulk Green's function of two isolated semi-infinite materials G_A and G_B, and the coupling between them across the interface, H_{AB} and H_{BA}. Following the works by García-Moliner *et al.* [51–53], we first introduce some projector operators that map the subspaces of different parts of the system. In particular, we define P as the projector of the space of the actual existing orbitals forming the system which is spanned by $P = P_A + P_B$. Within P there is an interface region with projector Γ consisting of two parts $\Gamma_A + \Gamma_B$. The bulk Hamiltonian $H_{A,B}$ and Green's functions $G_{A,B}$ are only meaningful in the corresponding parts of P and Γ.

Based on these projector operators, the interface Green's function G_I is given by [51–53]

$$\begin{aligned} G_I^{-1} = {} & [\Gamma_A\epsilon\Gamma_A - \Gamma_A H_A P_A G_A(\Gamma_A G_A \Gamma_A)^{-1}\Gamma_A] \\ & + [\Gamma_B\epsilon\Gamma_B - \Gamma_B H_B P_B G_B(\Gamma_B G_B \Gamma_B)^{-1}\Gamma_B] \\ & + (\Gamma_A H_I \Gamma_B + \Gamma_B H_I \Gamma_A). \end{aligned} \tag{17}$$

As the surface projection of any bulk Green's function $G_{A,B}$ gives the surface Green's function $g_{A,B}$, the above equation actually gives the surface Green's function matching formula for the interface region,

$$\begin{aligned} G_I(\epsilon,k_\parallel) &= \begin{pmatrix} g_A^{-1} & -H_{AB} \\ -H_{BA} & g_B^{-1} \end{pmatrix}^{-1} \\ &= \begin{pmatrix} \epsilon - H_{00}^A - \left(H_{01}^A\right)^\dagger \bar{T}^A & -H_{AB} \\ -H_{BA} & \epsilon - H_{00}^B - H_{01}^B T^B \end{pmatrix}^{-1}. \end{aligned} \tag{18}$$

Once the interface Green's function is known, the charge local density of states (LDOS) and spin LDOS [54] are given

straightforwardly with the expression

$$N_n(E,k_\parallel) = -\frac{1}{\pi}\mathrm{Im}[\mathrm{Tr}G^n(E+i\eta,k_\parallel)] \quad (19)$$

and

$$\mathbf{S}_n(E,k_\parallel) = -\frac{1}{\pi}\mathrm{Im}[\mathrm{Tr}G^n(E+i\eta,k_\parallel)\vec{\sigma}], \quad (20)$$

respectively, where $\vec{\sigma}$ are three spin operators in the local orbital basis and n is the principal layer index.

IV. RESULTS AND DISCUSSIONS

In this section, we present the interface states between QSH and several kinds of QAH insulators. For the single-valley QAH phase with $\mathcal{C} = 1$ in Sec. IV A, the electronic structure as well as the evolution of edge states with respect to the strength of the exchange field and the interface coupling are investigated. While these ones for a multivalley QAH state with a high Chern number and a valley-polarized QAH state are discussed in Secs. IV B and IV C, using the generalized Kane-Mele model. We also preform first-principles calculations for known material systems in Sec. IV D.

A. Singe valley QAH state with $\mathcal{C} = 1$

Firstly, we consider the interface between QSH and single-valley QAH states using the BHZ-type TB model that has been introduced in Sec. III A. With TB model parameters obtained by fitting the *ab initio* band structures [23], we can investigate the interface between half- and fully halogenated stanenes, which are QAH and QSH insulators, respectively [23,42].

We start from a junction system of two identical QSH insulators and consider the effect of a topological phase transition from a QSH to a QAH state on one side of the interface by increasing the amplitude of Zeeman-type term α_B in the right side and then α_A in the left side [Fig. 3(a)]. The LDOS of the interface region is shown in Fig. 3, from which we can clearly see the evolution of interface electronic structures. When $\alpha_A = \alpha_B = 0.0$, the whole system is in the QSH phase with a band gap. By increasing α_B, the bulk gap decreases gradually and closes at $\alpha_B \approx 0.5$ where a TPT happens as shown in Figs. 3(b)–3(d). Further increasing α_B, the bulk gap reopens leaving a gapless state connecting the conduction bands with valence bands. This is because the Zeeman-type term (i.e., the exchange field) drives the right semi-infinite system into the QAH phase, while the left one is still in the QSH phase. As a QSH insulator cannot be adiabatically connected to a QAH insulator without a gap closure due to the difference in topology, there must be a gapless state at the interface between them. However, if we keep $\alpha_B = 1.0$ and increase α_A from 0.0 to 1.0, the bulk band gap closes and reopens again, signaling another TPT [Figs. 3(f)–3(j)]. The whole system finally enters the QAH phase and the gapless interface state vanishes. Our result is in agreement with the analysis in Sec. II, unambiguously identifying the existence of a conducting interface state between QSH and QAH insulators.

Experimentally, the above process can be realized in functionalized stanene. Since the full and half-side halogenated stanene were found by previous studies [23,42] to be a QSH and a QAH insulator, respectively, one can tune the strength of the exchange field by gradually removing the halide atoms from one side of the halogenated stanene while keeping the other side halogenated. Then, the interface and corresponding gapless state between QSH and QAH phases would appear in this system, which might be probably observed by angle-resolved photoelectron spectroscopy or other measurements.

It is known that the topological edge states of QAH and QSH insulators are exponentially localized on the boundary, which is important for its practical applications. In order to characterize the localization of the interface state, we calculate the LDOS of several principal layers near the interface in the same energy and **k**-space range. As shown in Fig. 4, the gapless states within the bulk gap are localized in the interface region and decay rapidly away from the interface.

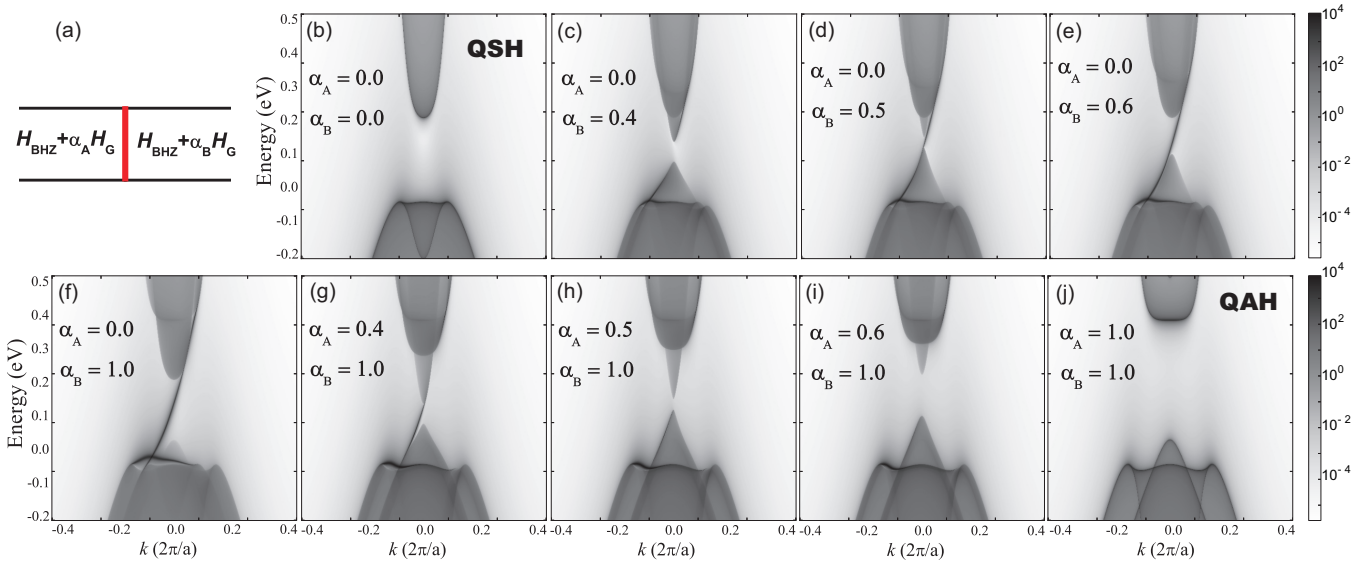

FIG. 3. (Color online) (a) The schematic of the calculated system. (b)-(j) LDOS of the interface between semi-infinite QSH and single-valley QAH insulators vs the strength of Zeeman term α_A and α_B.

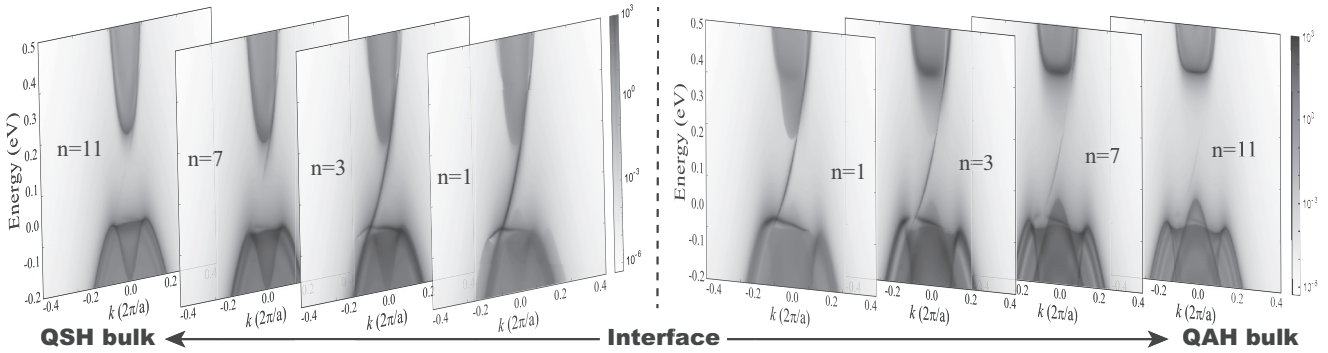

FIG. 4. Layer-resolved LDOS of the QSH/QAH interface state as a function of the principal layers index.

In particular, the signature of interface states almost vanishes within seven principal layers, similar to the edge states of QAH and QSH phases in this TB model. Although the edge and the interface states are of nearly equal decay length, edge reconstruction or decoration can significantly change the decaying behaviors of edge states and hence affect the amplitude for interedge tunneling and the performance of TS-based electronic devices [33,34]. On the contrary, the junction structure of the interface system provides a physical protection against those perturbations for the localized interface state, which may be of practical use in designing TS-based electronic devices with high performance and stability.

To better understand the evolution from edge states of QAH and QSH insulators to the interface state between them, we simulate the transition from two separate edges to a joint interface. To do this, we scale the TB Hamiltonian elements [H_{AB} and H_{BA} in Eq. (18)] that mediate the hopping between the two materials by a factor κ, with $\kappa = 0$ ($\kappa = 1$) for zero (full) coupling. And we calculate the spin LDOS of the two 0th principal layers of the QSH and QAH parts in the interface region separately (see Fig. 2) using Eq. (20). For $\kappa = 0.0$, corresponding to the two edges separated far enough without coupling, we find the helical and chiral edge states for QSH and QAH insulators, respectively, both of which are spin-polarized and bridge the fundamental band gap [Figs. 5(a) and 5(b)]. Upon the approach of the two semi-infinite systems (simulated by increasing κ to 1.0), two spin-down edge states couple to each other, open a gap at the crossing point and finally merge with the bulk-state continuum [Figs. 5(c)–5(j)]. But the spin-up edge state of QSH insulator "survives" in the formation of the interface and gradually permeates into the opposite side, as shown in Fig. 5. More precisely, the dispersion of the spin-up edge state does not change significantly with κ because no states with the same spin polarization could be coupled. The evolution of edge states confirms that the interface state in this system arises from the hybridization of the edge states of the QSH and QAH phases, which should be robust against any local perturbations.

B. Multivalley high-Chern-number QAH state with $\mathcal{C} = 2$

It is previously known that the number of edge states is equal to the absolute value of the Chern number due to the bulk-edge correspondence [4,5,55]. For QAH with a high Chern number ($|\mathcal{C}| \geqslant 2$), there are two or more chiral edge states. However, there are only two helical edge states with opposite spin polarizations at the edge of QSH insulators. How these edge states hybridize when the edges of QAH and QSH insulators approach each other? Does any localized state exist at the interface between QAH and QSH insulators? If yes, how many interface states exist in the bulk band gap? To answer these questions, we simulate the interface between QSH and multivalley high-Chern-number QAH (HQAH) states using the generalized Kane-Mele model outlined in Sec. III A. By switching off or on the exchange field parameter M we can drive the model into QSH or HQAH with $\mathcal{C} = 2$ based on the parameters listed in Table I.

We calculate the electronic structure and its evolution with scaling factor κ for the interface region, as shown in Fig. 6. For the uncoupled subsystems, we find the established 1D Dirac states of the QSH part and two chiral edge states of the HQAH part with $\mathcal{C} = 2$ [$\kappa = 0.0$, panel (a) in Fig. 6]. For clarity, we mark the spin polarization of all edge and interface states [Figs. 6(a) and 6(e)]. The helical QSH edge states consist of two gapless states connecting conduction and valance bands at different valleys (K and K'), while the two chiral QAH edge states are of the same spin polarization and located within the K or K' valley separately. Increasing the scaling factor κ opens up band gaps at the crossing points of edge states with the same spin polarization [Fig. 6(b)], leaving only two gapless states connecting bulk bands at different valleys. What is more, these states can hybridize with each other to change their dispersions in momentum space and mix their spin polarization, showing complicated evolution behavior comparing with the above case of $\mathcal{C} = 1$. Further increasing κ, one interface state is shifted upward into the conduction bands while the other state is shifted downward into the valence bands [Figs. 6(c) and 6(d)]. So one gapless state moves to the K valley and the other moves to the K' valley gradually. Finally, for full coupling, $\kappa = 1.0$, two interface states with opposite spin polarizations are left in the bulk band gap [Fig. 6(e)]. These results are essentially consistent with the theoretical analysis of Sec. II, because two spin-down edge states propagating in opposite directions (one from the QSH side and one from the HQAH side) couple to each other and vanish as κ increases, leaving a spin-up state from the QSH part and a remaining spin-down state from the HQAH part in the bulk band gap [see Fig. 6(f)].

More interestingly, the two interface states with opposite spin polarizations are located in different valleys with large

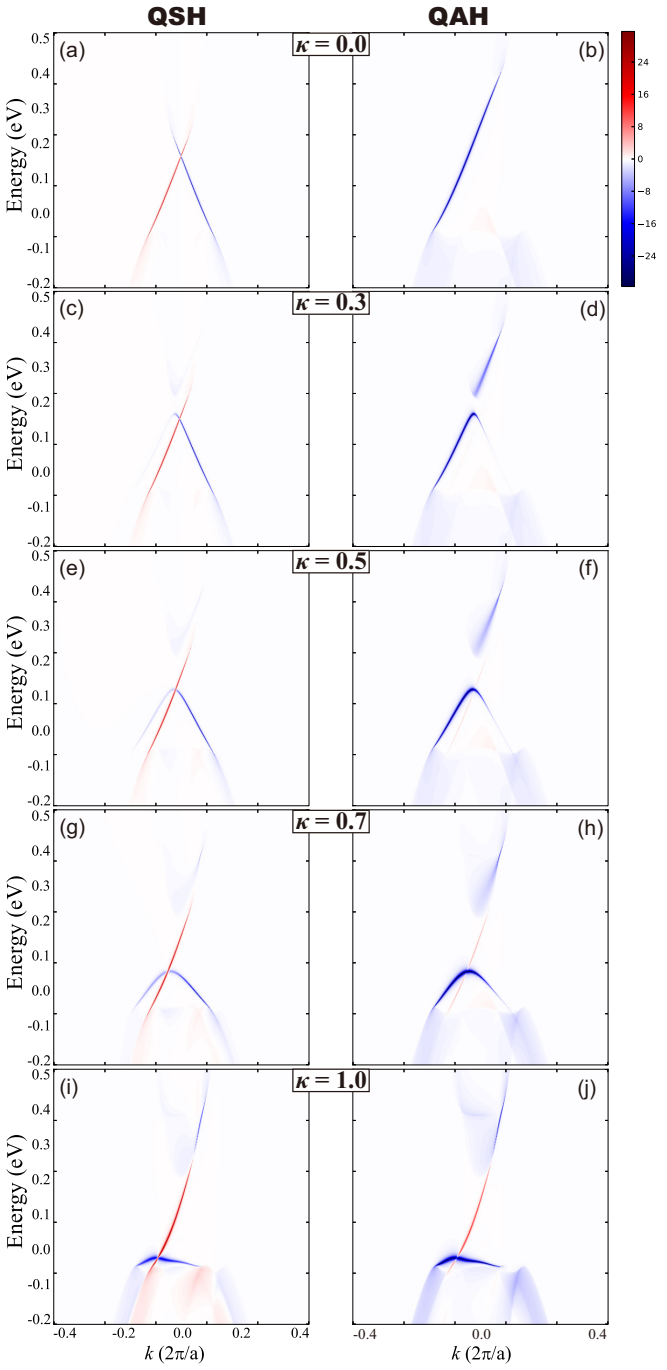

FIG. 5. (Color online) Spin-resolved electronic structures of the outmost principal layer (i.e., the 0th layer) of QSH (left panel) and QAH (right panel) parts in the interface system. The scaling factor κ increases from top to bottom ($\kappa = 0.0$ uncoupled; $\kappa = 1.0$ fully coupled). Different colors represent S_z along different directions (red and blue represent the $+z$ and $-z$ directions, respectively). The spin LDOS of S_z is depicted as a color scale.

separation in momentum space [56]. In other words, the formation of QSH/HQAH interface leads to valley-contrasting spin polarization of interface states. The coupling of spin and valley physics at the interface makes it possible to distinguish the valley degree of freedom by controlling the spin degree of freedom.

C. Valley-polarized QAH state with $\mathcal{C} = -1$

Valley-polarized QAH (VQAH) phase is a quantum state that exhibits the electronic properties of both the quantum valley Hall state and QAH state [40,41]. This novel topologically nontrivial state is characterized by a Chern number $\mathcal{C} = -1$ and a valley Chern number $\mathcal{C}_v = 3$. On the boundary of the VQAH insulator, there are two chiral edge states from the K' valley propagating in opposite directions to the only one edge state from the K valley. Due to the large separation of the two valleys in momentum space, the edge states are robust against intravalley scattering. However, in the presence of short-range disorder, intervalley scattering is inevitable and the edge state from the K valley can be easily scattered back to an edge state from the K' valley. Consequently, one pair of counterpropagating edge states (one from the K valley and the other from the K' valley) are destroyed, leaving only one chiral edge state from the K' valley, as required by the total Chern number $\mathcal{C} = -1$. Therefore we expect that the behavior of electrons in the QSH/VQAH interface is similar to that of QSH/QAH interface in Sec. IV A.

To demonstrate the conjecture, we calculate the electronic structures of the QSH/VQAH interface using the generalized Kane-Mele model described in Sec. III A with parameters listed in Table I. At the beginning ($\kappa = 0.0$), one gapless state connects conduction bands with valance bands at the K valley, whereas two gapless states with opposite spin polarizations are at the K' valley [Fig. 7(a)], which is consistent with previous works of the VQAH insulator [41]. On the contrary, the helical states of the QSH part connect conduction and valance bands at different valleys. Surprisingly, we find that a gap opens at the Dirac point of the helical QSH edge states when increasing the scaling factor κ [Fig. 7(b)]. This is distinct from the cases in Secs. IV A and IV B where gaps open at the crossing point of hybridized edge states from opposite sides of the interface. Moreover, both upper and lower parts of the detached Dirac cone move towards the K' valley and eventually merge into bulk bands as the interface coupling strength increases [Figs. 7(c) and 7(d)]. It seems that the edge states of the VQAH state are not affected during the process. However, the spin polarization of one edge state at the K' valley changes when $\kappa = 1.0$ [see Fig. 7(e)]. This is not surprising, as we will explain in an intuitional way as shown in Fig. 7(f). When the two semi-infinite subsystems approach one another, the two counterpropagating spin-up edge states [red arrows in Fig. 7(f)] interact with each other and vanish gradually, leaving only spin-down states at the interface. Actually, if we neglect the pair of VQAH edge states, which can be removed by intervalley scattering (dashed-line arrows in Fig. 7), the situation is almost the same as the case of $\mathcal{C} = 1$ in Sec. IV A

TABLE I. Parameters of the generalized Kane-Mele model (14) in different topological phases (in unit of the hopping energy t) [40].

Topological phase	λ_{SO}	λ_{IR}	λ_{ER}	λ_v	M[a]
HQAH ($\mathcal{C} = 2$)	0.02	0.08	0.01	0.0	0.5
VQAH ($\mathcal{C} = -1$)	0.07	0.08	0.05	0.0	0.5

[a]By reducing M to 0 and keeping other parameters unchanged, we can drive this model into the QSH phase.

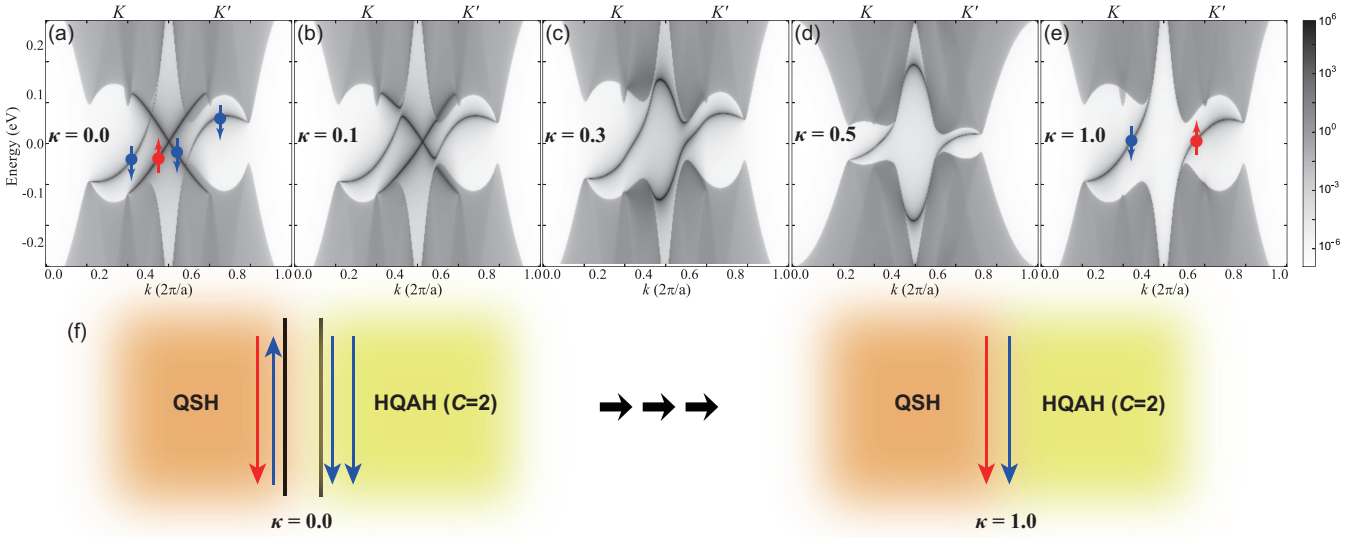

FIG. 6. (Color online) (a)–(e) LDOS of the QSH/HQAH interface region as a function of κ. The average spin LDOS of S_z is marked for all gapless states in (a) and (e). (f) Schematic of the spatial distribution of the edge (interface) channels at $\kappa = 0.0$ ($\kappa = 1.0$).

except that the remaining gapless channel is valley-polarized and could serve as a valley filter [41].

D. Hydrogenated bismuth (111) thin film: a first-principles study

We further investigate the QSH/QAH interface state in realistic material systems, i.e., the interface between fully and semihydrogenated Bi (111) thin film [see Fig. 8(a)]. Firstly, we construct 16-band *ab initio* TB models for H-Bi(111) and sH-Bi(111) in a Wannier basis, including all the Bi *s* and *p* valence orbitals. The effective TB Hamiltonian matrix elements of the interface system are then obtained directly from the two bulk Wannier Hamiltonians. Finally, we implement the interface Green's function method to obtain the LDOS of the interface region. It is worth noting that when generating the Wannier functions for the interface treatment, the Wannier basis function should be chosen as similar as possible for the two systems before constructing the interface Hamiltonian. Only in this way will the coupling Hamiltonian between the two materials through the interface be well defined. We therefore use the projected atomiclike WFs without applying a maximal-localization procedure [46]. The valence bands maxima of the two bulk systems have been aligned to the common Fermi level in the interface system, in accordance with the vacuum energy level.

Although the *ab initio* TB parameters using Wannier functions at the surface or interface are taken from bulk values, the edge electronic structures agree with the direct DFT results reported earlier [24]. As shown in Fig. 8(b), there is a pair of helical states at the edge of H-Bi(111), indicating that it is a QSH insulator. Whereas for sH-Bi(111), which is a valley-

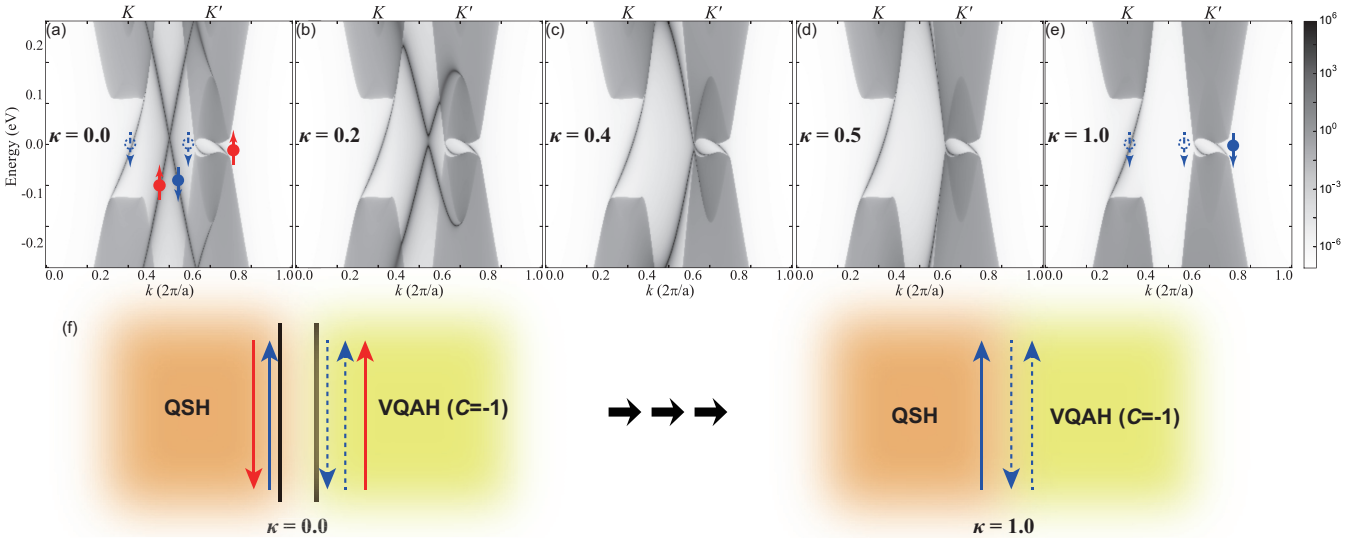

FIG. 7. (Color online) (a)–(e) LDOS of the QSH/VQAH interface region as a function of κ. The average spin LDOS of S_z is marked for each gapless states in (a) and (e). (f) Schematic figure of the spatial distribution of the edge (interface) channels at $\kappa = 0.0$ ($\kappa = 1.0$). The pair of gapless states which would vanish in the presence of intervalley scattering are labeled by a dashed-line arrow.

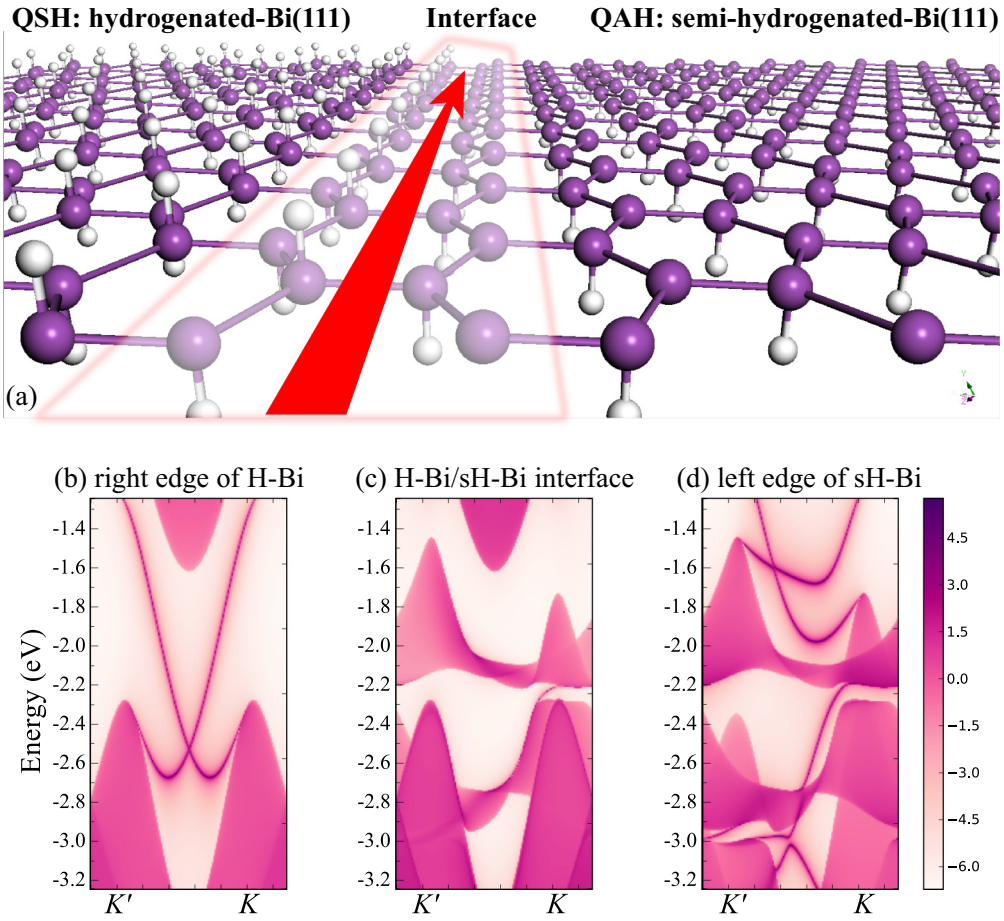

FIG. 8. (Color online) (a) A schematic illustration showing the QSH/QAH interface state between the fully and semihydrogenated Bi (111) films. (b) The helical edge state of H-Bi(111), (c) the QSH/QAH interface state between H-Bi(111) and sH-Bi(111), and (d) the chiral edge state of sH-Bi(111).

polarized QAH insulator with $\mathcal{C} = 1$, a chiral edge state exists around the K valley [Fig. 8(d)]. For the H-Bi(111)/sH-Bi(111) interface, a gapless state exists at the band gap as shown in Fig. 8(c). More importantly, the interface state is around the K valley, namely is valley-polarized, hence could be a good candidate for designing dissipationless valleytronics. These results again confirm the existence of the QSH/QAH interface state.

V. SUMMARY

In summary, we have studied the gapless states at the QSH/QAH interface using theoretical analysis and numerical calculations. We find that a chiral gapless state exists at the QSH/QAH interface, which does not simply inherit from the chiral edge states of QAH insulators. In fact, a chiral QAH edge state is typically destroyed due to the coupling to one of the helical edge states of a QSH insulator, when the two subsystems approach each other. Hence the "survived" chiral interface state stems from TR symmetry protected helical edge states of QSH insulators, and usually has an opposite spin polarization to the original chiral edge states of QAH insulators. Based on TB models, we systemically investigate the interfaces between QSH and different kinds of QAH insulators, including single-valley QAH, multivalley high-Chern-number QAH, and valley-polarized QAH insulators. The existence and distinct behaviors of the interface states are observed in all cases. In addition, we have used first-principles calculations to simulate the QSH/QAH interface in realistic material systems [i.e., hydrogenated Bi (111) bilayer], confirming the conclusions from the TB models.

Unlike the edge states of QSH or QAH insulators, which are significantly affected by edge defects, reconstruction and chemical decoration, the interface state is robust against these perturbations. Since the interface states are deeply buried between two bulk materials, the physical protection makes the interface state more stable and insensitive than topological edge states, which is important for enhancing the performance and stability of topological electronic devices in real environment.

ACKNOWLEDGMENTS

We thank Guo Li for valuable discussions. The work is supported by the Ministry of Science and Technology of China (Grants No. 2011CB606405 and No. 2011CB921901) and the National Natural Science Foundation of China (Grant No. 11334006). The calculations were done on the "Explorer 100" cluster system of Tsinghua University.

APPENDIX A: THE QSH/QAH INTERFACE STATE FROM THE BHZ MODEL ANALYSIS

In the following, we give a detailed analysis of the wave function connection at the QSH/QAH interface. From Eq. (7), we can easily get

$$\lambda_1^2+\lambda_2^2=2k_x^2+2F \quad \text{and} \quad \lambda_1^2\lambda_2^2=\frac{M^2-E^2}{B_-B_+}, \tag{A1}$$

where $F(M,E)=\dfrac{A^2-B_-(M-E)-B_+(M+E)}{2B_-B_+}$. Since $\lambda_{1,2}$ should be positive for $y<0$ region, the equation can be further reduced into

$$\lambda_1+\lambda_2=\sqrt{2k_x^2+2F+2\theta}, \tag{A2}$$

where $\theta(M,E)=\lambda_1\lambda_2=\sqrt{\frac{M^2-E^2}{B_-B_+}}$. Similarly, for $y>0$, we get

$$\lambda_1'+\lambda_2'=\sqrt{2k_x^2+2F'+2\theta'}, \tag{A3}$$

where $F'=F(M',E-S)$, $\theta'=\theta(M',E-S)$, $M'=M+(G_E-G_H)/2$, and $S=(G_E+G_H)/2$.

For simplicity, let us define the left side of Eq. (12) as a function $\Omega(E)$:

$$\begin{aligned}\Omega(E)=&(\sqrt{F+\theta}+\sqrt{F'+\theta'})^2[(M'+S-E)\theta+(M-E)\theta']\\&+\frac{BS-D(M'-M)}{B_-B_+}[(M'+S-E)\theta-(M-E)\theta'].\end{aligned} \tag{A4}$$

Hence solving Eq. (12) is equivalent to determining zero points of the function $\Omega(E)$. As the whole system should be insulating, the interface state (if exists) should lie in the bulk gap, bridging conduction and valance bands. Therefore the energy range we should consider [i.e., the domain of $\Omega(E)$] is just the bulk energy gap of the interface system. If $\Omega(E)$ has a zero point in the gap, one interface state should exist. However, if no zero point exists, it is evident that no interface state exists in the whole energy gap, due to the fact that the BHZ model is just a single-valley model.

Before proceeding with the detailed proof, we first mention certain restrictions on $S\pm M'$ and M to ensure that the domain of the function $\Omega(E)$ is not empty, which can be obtained by noting that

$$\lambda_1^2\lambda_2^2=\frac{M^2-E^2}{B_-B_+}>0, \quad \lambda_1'^2\lambda_2'^2=\frac{M'^2-(E-S)^2}{B_-B_+}>0. \tag{A5}$$

Physically, these restrictions just mean that the whole interface system is still an insulator rather than a metal and that the interface state should lie in the bulk energy gap. In other words, E should lie both in the QSH gap $[-|M|,|M|]$ and in the QAH gap $[\min(G_E+M,G_H-M),\max(G_E+M,G_H-M)]$ (i.e., $[S-|M'|,S+|M'|]$). Hence the intersection of these two sets must not be empty, i.e.,

$$S-|M'|<|M|, \quad -|M|<S+|M'|. \tag{A6}$$

The interval of the insulating gap for the whole interface system is thus determined by the relative value of $\pm M$ and $S\pm M'$.

Obviously, it is extremely difficult to directly calculate the zero points of $\Omega(E)$, which is in fact unnecessary. Since only the existence of the zero points is important rather than the specific values of them, we adopt an indirect method here. The basic idea of the method is to evaluate the existence of zero points of $\Omega(E)$ inside the gap through its behavior on the boundary of the gap. This is not straightforward. To clarify the method, let us first look at a simple example: supposing $f(x)$ is a continuous function on the interval $[a,b]$, if $f(a)>0$, $f(b)=0$, and $\dot{f}(b)>0$ as shown in Fig. 9(a), we can assert

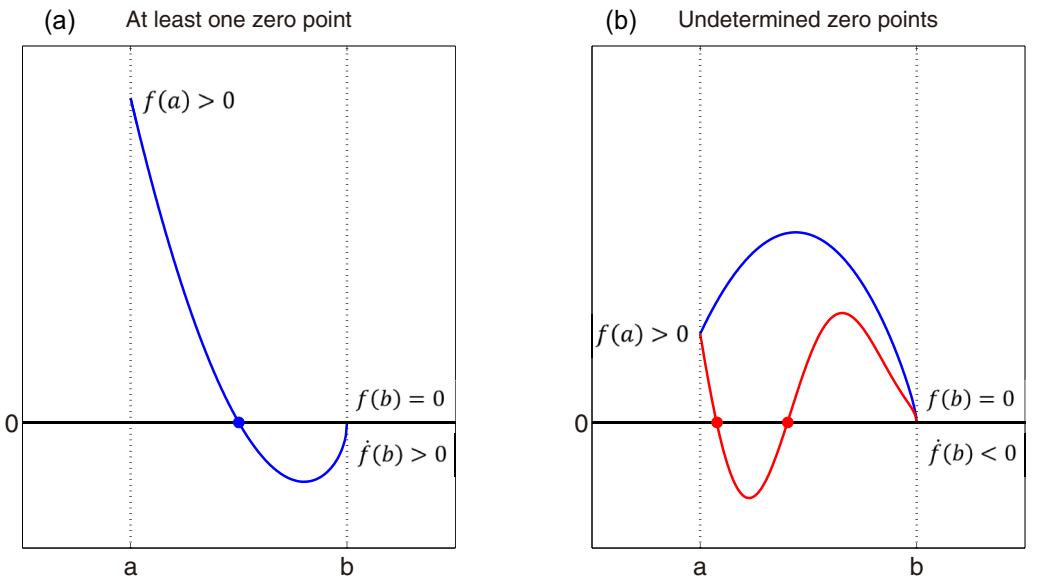

FIG. 9. (Color online) Schematic illustration of the simple example. (a) In the first case where $f(a)>0$, $f(b)=0$, and $\dot{f}(b)>0$, there must be at least one zero point. (b) In the second case where $f(a)>0$, $f(b)=0$, and $\dot{f}(b)<0$, the existence of zero points cannot be determined directly.

that $f(x)$ must have at least one zero point on $[a,b]$ due to the continuity requirements of $f(x)$. Although there are certain situations where the existence of zero points cannot be decided directly [for example, $f(a) > 0$, $f(b) = 0$, and $\dot{f}(b) < 0$, see Fig. 9(b)], still a lot of information can be obtained by this method. And for those exceptional cases, a different method will be adopted to demonstrate the existence of zero points.

Because the relative values of $\pm M$ and $S \pm M'$ are not assumed yet, the boundary of the insulating gap is not determined. Hence we derive behaviors of $\Omega(E)$ at $E = \pm M$ and $S \pm M'$ first. After that, different possibilities of their relative values are discussed separately. Since $\Omega(M) = \Omega(S + M') = 0$, all we need to derive are just the signs of the following four quantities:

$$\Omega(S - M'), \quad \Omega(-M), \quad \dot{\Omega}(S + M') \quad \text{and} \quad \dot{\Omega}(M), \tag{A7}$$

where $\dot{\Omega}(E) = \mathrm{d}\,\Omega(E)/\mathrm{d}E$ is the derivative.

By direct calculation, it is easy to get

$$\begin{aligned}\Omega(S - M') &= 2M'\theta\left[(\sqrt{F+\theta} + \sqrt{F'+\theta'})^2 + \frac{BS - D(M' - M)}{B_- B_+}\right],\\ \Omega(-M) &= 2M\theta'\left[(\sqrt{F+\theta} + \sqrt{F'+\theta'})^2 - \frac{BS - D(M' - M)}{B_- B_+}\right].\end{aligned} \tag{A8}$$

For convenience, in the following, we will proceed with a simplifying assumption that A is large enough (roughly speaking), so that F and F' are large enough, to ensure that

$$(\sqrt{F+\theta} + \sqrt{F'+\theta'})^2 > \left|\frac{BS - D(M' - M)}{B_- B_+}\right| \tag{A9}$$

for all possible values of E in the bulk energy gap. Further discussions about this restriction on A will be given later (see Appendix B). Using this restriction, we have

$$\Omega(S - M') \sim M', \quad \Omega(-M) \sim M. \tag{A10}$$

Here, "$\sim$" means having the same sign.

To get the derivative $\dot{\Omega}(E)$, it is convenient to use the following relations:

$$\frac{\partial F}{\partial E} = \frac{\partial F'}{\partial E} = -\frac{D}{B_- B_+}, \quad \frac{\partial \theta}{\partial E} = -\frac{E}{\theta B_- B_+} \quad \text{and} \quad \frac{\partial \theta'}{\partial E} = -\frac{E - S}{\theta' B_- B_+}. \tag{A11}$$

Then we get

$$\begin{aligned}\dot{\Omega}(E) = &\left(\frac{-D - \frac{E}{\theta}}{B_+ B_- \sqrt{F+\theta}} + \frac{-D - \frac{E-S}{\theta'}}{B_+ B_- \sqrt{F'+\theta'}}\right)(\sqrt{F+\theta} + \sqrt{F'+\theta'})[(M' + S - E)\theta + (M - E)\theta']\\ &+ (\sqrt{F+\theta} + \sqrt{F'+\theta'})^2\left[(M' + S - E)\frac{-E}{\theta B_- B_+} + (M - E)\frac{S - E}{\theta' B_- B_+} - (\theta + \theta')\right]\\ &+ \frac{BS - D(M' - M)}{B_- B_+}\left[(M' + S - E)\frac{-E}{\theta B_- B_+} - (M - E)\frac{S - E}{\theta' B_- B_+} + (\theta' - \theta)\right].\end{aligned} \tag{A12}$$

Note that the derivative $\dot{\Omega}(E)$ is divergent at $E = S + M'$ and M. Because we just care about the sign of $\dot{\Omega}(E)$, we take the limit and leave out all the finite terms, which yields

$$\begin{aligned}\dot{\Omega}(S + M') &= \frac{M'}{B_+ B_-}(S + M' - M)\left[(\sqrt{F+\theta} + \sqrt{F'+\theta'})^2 - \frac{BS - D(M' - M)}{B_- B_+}\right]\frac{1}{0^+},\\ \dot{\Omega}(M) &= -\frac{M}{B_+ B_-}(S + M' - M)\left[(\sqrt{F+\theta} + \sqrt{F'+\theta'})^2 + \frac{BS - D(M' - M)}{B_- B_+}\right]\frac{1}{0^+}.\end{aligned} \tag{A13}$$

Due to the restriction (A9) on A, it is readily seen that

$$\dot{\Omega}(S + M') \sim M'(S + M' - M), \quad \dot{\Omega}(M) \sim -M(S + M' - M). \tag{A14}$$

Equations (A10) and (A14) play a critical role in deciding the existence/absence of the interface state as shown in the following discussion.

Now, let us determine the signs of the four quantities in Eq. (A7) in different cases according to Eqs. (A10) and (A14). First of all, we consider the $MM' < 0$ case where either $M' < 0 < M$ or $M < 0 < M'$ is valid. According to Eq. (A6), we know that $S + M' - M \sim M'$ in both cases. Therefore $\dot{\Omega}(S + M') \sim M'M' > 0$ and $\dot{\Omega}(M) \sim -MM' > 0$ [see Eq. (A14)]. Combining with Eq. (A10): $\Omega(S - M') \sim M'$, $\Omega(-M) \sim M$, we thus can determine the existence of an interface state in all possible situations. (1) $M' < 0 < M$, $S + M' < -M < M < S - M'$. The interval of the energy gap is $[-M, M]$. Since $\Omega(-M) > 0$, $\dot{\Omega}(M) > 0$ and $\Omega(M) = 0$, there must be zero points in $[-M, M]$.

(2) $M' < 0 < M, S + M' < -M < S - M' < M$. The interval of the energy gap is $[-M, S - M']$. Since $\Omega(-M) > 0, \Omega(S - M') < 0$, there must be zero points in $[-M, S - M']$.

(3) $M' < 0 < M, -M < S + M' < S - M' < M$. The interval of the energy gap is $[S + M', S - M']$. Since $\dot{\Omega}(S + M') > 0$, $\Omega(S - M') < 0$, and $\Omega(S + M') = 0$, there must be zero points in $[S + M', S - M']$.

(4) $M' < 0 < M, -M < S + M' < M < S - M'$. The interval of the energy gap is $[S + M', M]$. Since $\dot{\Omega}(S + M') > 0$, $\dot{\Omega}(M) > 0$, and $\Omega(M) = 0$, as well as $\Omega(S + M') = 0$, there must be zero points in $[S + M', M]$.

(5) $M < 0 < M', S - M' < M < -M < S + M'$. The interval of the energy gap is $[M, -M]$. Since $\Omega(-M) < 0, \dot{\Omega}(M) > 0$, and $\Omega(M) = 0$, there must be zero points in $[M, -M]$.

(6) $M < 0 < M', S - M' < M < S + M' < -M$. The interval of the energy gap is $[M, S + M']$. Since $\dot{\Omega}(M) > 0$, $\dot{\Omega}(S + M') > 0$, and $\Omega(M) = 0$, as well as $\Omega(S + M') = 0$, there must be zero points in $[M, S + M']$.

(7) $M < 0 < M', M < S - M' < -M < S + M'$. The interval of the energy gap is $[S - M', -M]$. Since $\Omega(-M) < 0$, $\Omega(S - M') > 0$, there must be zero points in $[S - M', -M]$.

(8) $M < 0 < M', M < S - M' < S + M' < -M$. The interval of the energy gap is $[S - M', S + M']$. Since $\Omega(S - M') > 0$, $\dot{\Omega}(S + M') > 0$, and $\Omega(S + M') = 0$, there must be zero points in $[S - M', S + M']$.

Thus we have proved that when $MM' < 0$, the interface state will always exist.

Now let us turn to the $MM' > 0$ case. Since the above method does not work in this case, we use a different method. We rewrite the original Eq. (12) as

$$(M' + S - E)\theta\left[(\sqrt{F + x} + \sqrt{F' + x'})^2 + \frac{BS - D(M' - M)}{B_- B_+}\right] + (M - E)\theta'\left[(\sqrt{F + x} + \sqrt{F' + x'})^2 - \frac{BS - D(M' - M)}{B_- B_+}\right] = 0. \tag{A15}$$

For $MM' > 0$, there are also two possible situations. (1) $M > 0$ and $M' > 0$. In this case, the restrictions from Eq. (A5) on E are $-M < E < M$ and $S - M' < E < S + M'$. It is easy to see that $M - E > 0$ and $M' + S - E > 0$. (2) $M < 0$ and $M' < 0$. Similarly, we have $M - E < 0$ and $M' + S - E < 0$. Therefore in both cases, we have $M' + S - E \sim M - E$. Note that in Eq. (A15), θ, θ', and expressions in square brackets are positive. Obviously, the left side of Eq. (A15) does not change sign as E varies in the bulk energy gap, clearly indicating that the equation does not have a solution. Thus no interface state exists when $MM' > 0$.

In conclusion, we have shown that if $MM' < 0$, an interface state exists; and if not, no such state exists for the upper block. For the lower block, we can perform a similar analysis. The only difference is that we should use $M'' = M - (G_E - G_H)/2$ and $S'' = -S$ instead of M' and S. After a very similar derivation, we conclude that the existence condition of interface states for the lower block is $MM'' < 0$.

Finally, we can consider the QSH/QAH interface based on the above conclusions. For the QAH side, Eqs. (3) and (4) must be satisfied, i.e.,

$$M'M'' < 0, \tag{A16}$$

$$(M + S)(M - S) > 0. \tag{A17}$$

Physically speaking, Eq. (A17) just ensures that the QAH system is in an insulating phase, while Eq. (A16) guarantees that either $MM' < 0, MM'' > 0$ or $MM' > 0, MM'' < 0$ is valid. Hence an interface state exists either in the spin-up or spin-down channel at the QSH/QAH interface.

APPENDIX B: DISCUSSIONS ABOUT THE RESTRICTION ON THE PARAMETER *A*

As mentioned above, we make a simplifying assumption that the parameter A is large enough to ensure Eq. (A9). Actually, A indeed satisfies the restriction in realistic materials described by the BHZ model [3]. As a parameter of the BHZ model, A already meets certain conditions to ensure that the model can describe correct topological phases. For example, in an previous analytical study of the BHZ model, Zhou *et al.* [38] showed that A in fact satisfies the following restriction, which is not mentioned in the original BHZ model [3],

$$\frac{A^2}{B_+ B_-} > \frac{4M}{B} > 0, \tag{B1}$$

to guarantee the existence of topological edge states.

As Eq. (A9) should be valid for all allowed values of E in the bulk energy gap, here we derive a possible condition for A:

$$A > \sqrt{\Sigma(\sqrt{|B_-|} + \sqrt{|B_+|})^2 + \frac{|B||S| + 2|D|\Sigma}{2}}, \tag{B2}$$

where $\Sigma = \max(2|M|, |M - S + M'|, |M + S - M'|)$. This condition is indeed satisfied by the parameters of HgTe/CdTe quantum wells [3].

[1] F. D. M. Haldane, Phys. Rev. Lett. **61**, 2015 (1988).

[2] C. L. Kane and E. J. Mele, Phys. Rev. Lett. **95**, 226801 (2005); **95**, 146802 (2005).

[3] B. A. Bernevig, T. L. Hughes, and S.-C. Zhang, Science **314**, 1757 (2006); M. König, S. Wiedmann, C. Brüne, A. Roth, H. Buhmann, L. W. Molenkamp, X.-L. Qi, and S.-C. Zhang, *ibid.* **318**, 766 (2007).

[4] B. I. Halperin, Phys. Rev. B **25**, 2185 (1982).

[5] Y. Hatsugai, Phys. Rev. Lett. **71**, 3697 (1993).

[6] K. v. Klitzing, G. Dorda, and M. Pepper, Phys. Rev. Lett. **45**, 494 (1980).

[7] R. Takahashi and S. Murakami, Phys. Rev. Lett. **107**, 166805 (2011).

[8] D. Sen and O. Deb, Phys. Rev. B **85**, 245402 (2012).

[9] C. De Beule and B. Partoens, Phys. Rev. B **87**, 115113 (2013).

[10] T. Habe and Y. Asano, Phys. Rev. B **88**, 155442 (2013).

[11] T. Rauch, M. Flieger, J. Henk, and I. Mertig, Phys. Rev. B **88**, 245120 (2013).

[12] C.-X. Liu, X.-L. Qi, X. Dai, Z. Fang, and S.-C. Zhang, Phys. Rev. Lett. **101**, 146802 (2008).

[13] R. Yu, W. Zhang, H.-J. Zhang, S.-C. Zhang, X. Dai, and Z. Fang, Science **329**, 61 (2010).

[14] Q.-Z. Wang, X. Liu, H.-J. Zhang, N. Samarth, S.-C. Zhang, and C.-X. Liu, Phys. Rev. Lett. **113**, 147201 (2014).

[15] H. Zhang, Y. Xu, J. Wang, K. Chang, and S.-C. Zhang, Phys. Rev. Lett. **112**, 216803 (2014).

[16] C.-Z. Chang, J. Zhang, X. Feng, J. Shen, Z. Zhang, M. Guo, K. Li, Y. Ou, P. Wei, L.-L. Wang, Z.-Q. Ji, Y. Feng, S. Ji, X. Chen, J. Jia, X. Dai, Z. Fang, S.-C. Zhang, K. He, Y. Wang, L. Lu, X.-C. Ma, and Q.-K. Xue, Science **340**, 167 (2013).

[17] R. Dingle, H. L. Störmer, A. C. Gossard, and W. Wiegmann, Appl. Phys. Lett. **33**, 665 (1978).

[18] E. F. Schubert, J. Vac. Sci. Technol. A **8**, 2980 (1990).

[19] J. Ding, Z. Qiao, W. Feng, Y. Yao, and Q. Niu, Phys. Rev. B **84**, 195444 (2011).

[20] H. Zhang, C. Lazo, S. Blügel, S. Heinze, and Y. Mokrousov, Phys. Rev. Lett. **108**, 056802 (2012).

[21] H. Jiang, Z. Qiao, H. Liu, J. Shi, and Q. Niu, Phys. Rev. Lett. **109**, 116803 (2012).

[22] J. Zhang, B. Zhao, and Z. Yang, Phys. Rev. B **88**, 165422 (2013).

[23] S.-C. Wu, G. Shan, and B. Yan, Phys. Rev. Lett. **113**, 256401 (2014).

[24] C. Niu, G. Bihlmayer, H. Zhang, D. Wortmann, S. Blügel, and Y. Mokrousov, Phys. Rev. B **91**, 041303 (2015).

[25] C.-C. Liu, J.-J. Zhou, and Y. Yao, Phys. Rev. B **91**, 165430 (2015).

[26] Y. Wang, X. Xu, J. Lu, M. Lin, Q. Bao, B. Özyilmaz, and K. P. Loh, ACS Nano **4**, 6146 (2010).

[27] L. Zhang, J. Yu, M. Yang, Q. Xie, H. Peng, and Z. Liu, Nat. Commun. **4**, 1443 (2013).

[28] D. Haberer, C. E. Giusca, Y. Wang, H. Sachdev, A. V. Fedorov, M. Farjam, S. A. Jafari, D. V. Vyalikh, D. Usachov, X. Liu, U. Treske, M. Grobosch, O. Vilkov, V. K. Adamchuk, S. Irle, S. R. P. Silva, M. Knupfer, B. Bchner, and A. Grneis, Adv. Mater. **23**, 4497 (2011).

[29] K. F. Garrity and D. Vanderbilt, Phys. Rev. Lett. **110**, 116802 (2013).

[30] Z. Qiao, W. Ren, H. Chen, L. Bellaiche, Z. Zhang, A. H. MacDonald, and Q. Niu, Phys. Rev. Lett. **112**, 116404 (2014).

[31] Z. Liu, C.-X. Liu, Y.-S. Wu, W.-H. Duan, F. Liu, and J. Wu, Phys. Rev. Lett. **107**, 136805 (2011).

[32] F. Yang, L. Miao, Z. F. Wang, M.-Y. Yao, F. Zhu, Y. R. Song, M.-X. Wang, J.-P. Xu, A. V. Fedorov, Z. Sun, G. B. Zhang, C. Liu, F. Liu, D. Qian, C. L. Gao, and J.-F. Jia, Phys. Rev. Lett. **109**, 016801 (2012).

[33] Z. F. Wang, L. Chen, and F. Liu, Nano Lett. **14**, 2879 (2014).

[34] X. Li, H. Liu, H. Jiang, F. Wang, and J. Feng, Phys. Rev. B **90**, 165412 (2014).

[35] F. Virot, R. Hayn, M. Richter, and J. van den Brink, Phys. Rev. Lett. **111**, 146803 (2013).

[36] S.-Y. Xu, Y. Xia, L. A. Wray, S. Jia, F. Meier, J. H. Dil, J. Osterwalder, B. Slomski, A. Bansil, H. Lin, R. J. Cava, and M. Z. Hasan, Science **332**, 560 (2011).

[37] T. Okuda, T. Maegawa, M. Ye, K. Shirai, T. Warashina, K. Miyamoto, K. Kuroda, M. Arita, Z. S. Aliev, I. R. Amiraslanov, M. B. Babanly, E. V. Chulkov, S. V. Eremeev, A. Kimura, H. Namatame, and M. Taniguchi, Phys. Rev. Lett. **111**, 206803 (2013).

[38] B. Zhou, H.-Z. Lu, R.-L. Chu, S.-Q. Shen, and Q. Niu, Phys. Rev. Lett. **101**, 246807 (2008).

[39] T.-W. Chen, Z.-R. Xiao, D.-W. Chiou, and G.-Y. Guo, Phys. Rev. B **84**, 165453 (2011).

[40] M. Ezawa, Phys. Rev. Lett. **109**, 055502 (2012).

[41] H. Pan, Z. Li, C.-C. Liu, G. Zhu, Z. Qiao, and Y. Yao, Phys. Rev. Lett. **112**, 106802 (2014); H. Pan, X. Li, H. Jiang, Y. Yao, and S. A. Yang, Phys. Rev. B **91**, 045404 (2015).

[42] Y. Xu, B. Yan, H.-J. Zhang, J. Wang, G. Xu, P. Tang, W. Duan, and S.-C. Zhang, Phys. Rev. Lett. **111**, 136804 (2013); P. Tang, P. Chen, W. Cao, H. Huang, S. Cahangirov, L. Xian, Y. Xu, S.-C. Zhang, W. Duan, and A. Rubio, Phys. Rev. B **90**, 121408 (2014).

[43] G. Kresse and J. Furthmüller, Comput. Mater. Sci. **6**, 15 (1996).

[44] J. P. Perdew, K. Burke, and M. Ernzerhof, Phys. Rev. Lett. **77**, 3865 (1996).

[45] A. A. Mostofi, J. R. Yates, Y.-S. Lee, I. Souza, D. Vanderbilt, and N. Marzari, Comput. Phys. Commun. **178**, 685 (2008).

[46] N. Marzari and D. Vanderbilt, Phys. Rev. B **56**, 12847 (1997); I. Souza, N. Marzari, and D. Vanderbilt, *ibid.* **65**, 035109 (2001).

[47] J. R. Yates, X. Wang, D. Vanderbilt, and I. Souza, Phys. Rev. B **75**, 195121 (2007).

[48] M. Kim, C. H. Kim, H.-S. Kim, and J. Ihm, Proc. Natl. Acad. Sci. USA **109**, 671 (2012).

[49] H. Huang, J. Liu, and W. Duan, Phys. Rev. B **90**, 195105 (2014).

[50] M. P. López Sancho, J. M. López Sancho, and J. Rubio, J. Phys. F **14**, 1205 (1984); M. P. López Sancho, J. M. López Sancho, J. M. L. Sancho, and J. Rubio, *ibid.* **15**, 851 (1985).

[51] M. C. Mũoz, V. R. Velasco, and F. García-Moliner, Prog. Surf. Sci. **26**, 117 (1987).

[52] F. García-Moliner and V. R. Velasco, Phys. Rep. **200**, 83 (1991).

[53] F. García-Moliner and V. R. Velasco, *Theory of Single and Multiple Interfaces: The Method of Surface Green Function Matching* (World Scientific, Singapore, 1992).

[54] X. Dai, T. L. Hughes, X.-L. Qi, Z. Fang, and S.-C. Zhang, Phys. Rev. B **77**, 125319 (2008).

[55] H. Zhang, H. Huang, K. Haule, and D. Vanderbilt, Phys. Rev. B **90**, 165143 (2014).

[56] D. Xiao, W. Yao, and Q. Niu, Phys. Rev. Lett. **99**, 236809 (2007); D. Xiao, G.-B. Liu, W. Feng, X. Xu, and W. Yao, *ibid.* **108**, 196802 (2012).